

Where is SUSY?

C. Beskidt^a, W. de Boer^{a1}, D.I. Kazakov^{b,c}, F. Ratnikov^{a,c}

^a *Institut für Experimentelle Kernphysik, Karlsruhe Institute of Technology,
P.O. Box 6980, 76128 Karlsruhe, Germany*

^b *Bogoliubov Laboratory of Theoretical Physics, Joint Institute for Nuclear Research,
141980, 6 Joliot-Curie, Dubna, Moscow Region, Russia*

^c *Institute for Theoretical and Experimental Physics,
117218, 25 B.Cheremushkinskaya, Moscow, Russia*

Abstract

The direct searches for Supersymmetry at colliders can be complemented by direct searches for dark matter (DM) in underground experiments, if one assumes the Lightest Supersymmetric Particle (LSP) provides the dark matter of the universe. It will be shown that within the Constrained minimal Supersymmetric Model (CMSSM) the direct searches for DM are complementary to direct LHC searches for SUSY and Higgs particles using analytical formulae. A combined excluded region from LHC, WMAP and XENON100 will be provided, showing that within the CMSSM gluinos below 1 TeV and LSP masses below 160 GeV are excluded ($m_{1/2} > 400\text{GeV}$) independent of the squark masses.

1 Introduction

Supersymmetry (SUSY) is the leading candidate for physics beyond the SM, since the Lightest Supersymmetric Particle (LSP) has all the properties expected for the Weakly Interacting Massive Particles (WIMPs) of the dark matter [1–3], which is known to make up more than 80% of the matter in the universe [4]. Unfortunately, no supersymmetric particles have been observed so far, even at the highest energy of the LHC [5–17], nor have WIMPs been observed beyond doubt in elastic scattering of WIMPs on nuclei, as pursued with direct searches in underground detectors, like CDMS, EDELWEISS and XENON100, which give upper limits on the elastic scattering cross section typically between 10^{-43} and 10^{-44} cm² [18, 19]. The direct DM detection experiments, the search for SUSY and the search for Higgs particles all determine complementary excluded regions in the parameter space of supersymmetric models, like the Constrained Minimal Supersymmetric Model (CMSSM), see [20, 21] and reviews, e.g. [22–25]. In this model all the arguments in favour of Supersymmetry, like the unification of the coupling constants at the GUT (Grand Unified Theory) scale with SUSY masses in the TeV range [26] and electroweak symmetry breaking (EWSB) by radiative corrections [27, 28], are implemented. In the CMSSM one furthermore assumes that the masses of spin 0 (spin 1/2) particles

¹Email: wim.de.boer@kit.edu

are unified at the GUT scale with values $m_0(m_{1/2})$. So the many parameters of SUSY models are reduced to only 4: the two mass parameters $m_0, m_{1/2}$ and two parameters related to the Higgs sector: the trilinear coupling at the GUT scale A_0 , and $\tan\beta$, the ratio of the vacuum expectation values of the two neutral components of the two Higgs doublets. Electroweak symmetry breaking (EWSB) fixes the scale of μ , so only its sign is a free parameter. The positive sign is taken, as suggested by the small deviation of the SM prediction from the muon anomalous moment, see e.g. [29].

Within the CMSSM the direct searches for SUSY particles ("sparticles") at the LHC, the direct DM searches and the relic density, as obtained from cosmological observations, are related and one can combine them to see which region of the supersymmetric parameter space is excluded, if one includes all constraints. Such combinations have been pursued by many different groups either using a frequentist approach by maximizing a likelihood or using random sampling techniques of the parameter space, see e.g. [30–41] and references therein.

The sampling techniques are dependent on the prior, which leads to an additional, non-quantifiable uncertainty in the excluded or allowed regions, see e.g. [42] for a recent discussion and references therein. We believe this uncertainty is due to the high correlations between three of the four parameters, as we discussed in two previous papers: m_0 is highly correlated with $\tan\beta$ because of the relic density constraint, which requires large $\tan\beta$ in most of the parameter space except for the narrow co-annihilation regions at low and large m_0 [43] and the trilinear coupling is highly correlated with $\tan\beta$ because of heavy flavour constraints, notably the $B_s^0 \rightarrow \mu^+\mu^-$ constraint [44]. Note that $B_s^0 \rightarrow \mu^+\mu^-$ is not only proportional to $\tan^6\beta$, so it tends to become above the present upper limit for large $\tan\beta$, but it can be strongly reduced by the appropriate value of the trilinear coupling to values even below the SM value by negative interferences [44].

Such strong correlations lead to likelihood spikes in the parameter region, where three of the four parameters have to have specific correlated values. Although the likelihood of such narrow regions is high, they are either not found in methods based on stepping techniques or their probability is given a different weight because of its "low posterior mass". To cope with the strong correlations we use a multistep fitting technique, defined by fitting the parameters with the strongest correlation first, i.e. we fit first $\tan\beta$ and A_0 for each pair of the mass parameters m_0 and $m_{1/2}$ by minimizing the χ^2 with the program Minuit[45] or by using a Markov Chain Monte Carlo or multinest fitting technique to find the maximum likelihood, while integrating over the nuisance parameters. Both the χ^2 minimization and Markov Chain sampling of the parameter space give practical identical results in this multistep fitting technique and no prior dependence has been found, since for each point in the $(m_0, m_{1/2})$ grid there is a unique solution for $\tan\beta$, mainly from the relic density constraint, and A_0 can be fine-tuned to further minimize χ^2 . Furthermore the multistep fitting technique is fast, since initially only two parameters are fitted for each point in the $(m_0, m_{1/2})$ grid. Once the SUSY parameters have been fitted, one should also vary the SM parameters or marginalize over them, like the top and bottom mass and the strong coupling constant. However, these are highly correlated with the SUSY parameters, so if one repeats the fit with different values of the SM parameters or marginalizes over them one usually finds the same fit probability with slightly different values of the SUSY parameters. The SM parameters are given in the Particle Data Book [46]; we use $m_{top}^{pole} = 172.5 \pm 1.3$ and $m_b(m_b)^{\overline{MS}} = 4.25 \pm 0.2$ GeV for the heavy quark masses and $\alpha_s = 0.1172 \pm 0.02$ for the strong coupling constant.

All observables discussed below were calculated with the public code micrOMEGAs 2.4.1 [47, 48] combined with Suspect 2.41 as mass spectrum calculator [49].

The purpose of this letter is twofold: we show that the data from the LHC, WMAP and XENON100 lead to complementary excluded regions and discuss the reasons why by giving analytical approximations. We furthermore combine the newest data and show that a lower limit of $m_{1/2}$ of 400 GeV can be obtained independent of m_0 , which implies a lower limit of 160 GeV on the LSP and 1 TeV on the gluino. Our results differ from similar analysis referred to above and we discuss possible reasons. We start by discussing the observations and the excluded regions of each observation separately.

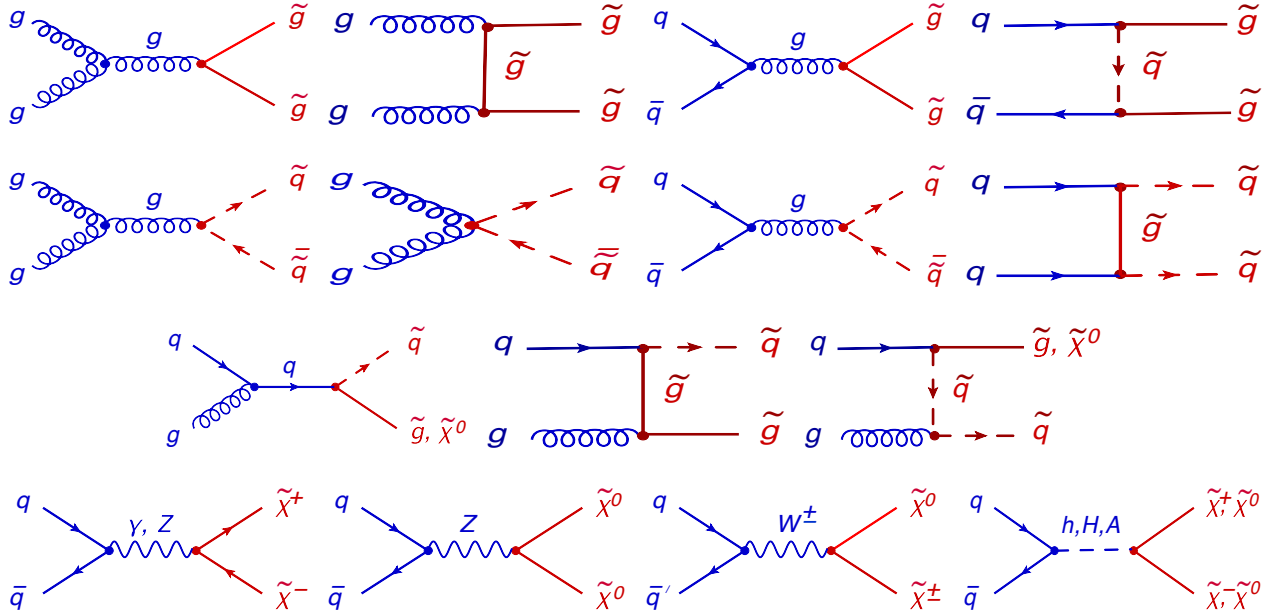


Figure 1: Examples of diagrams for SUSY particle production via strong interactions (top rows for $\tilde{g}\tilde{g}$, $\tilde{q}\tilde{q}$ and $\tilde{g}\tilde{q}$, respectively) and electroweak interactions (lowest row).

2 Excluded region by direct searches for SUSY at the LHC

In proton-proton collisions strongly interacting supersymmetric particles can be produced by the main diagrams shown in the first three rows of Fig. 1, while the main diagrams for the electroweak production are shown in the last row. The corresponding cross sections are shown in Fig. 2 for a centre-of-mass energy of 7 TeV. One observes that the cross section for the "strong" production of $\tilde{q}\tilde{q}$ and $\tilde{g}\tilde{g}$ are large for low values of m_0 and $m_{1/2}$, the gluino production $\tilde{g}\tilde{g}$ is strongest at small values of $m_{1/2}$ and the electroweak production of gauginos starts to increase at large values of m_0 . The reason for the increase of the electroweak production at large m_0 is the decrease of the Higgs mixing parameter μ , as determined from EWSB, which leads to a stronger mixing of the Higgsino component in the gauginos and so the coupling to the weak gauge bosons and Higgs bosons increases, thus increasing the amplitudes for the diagrams in the last row of Fig. 1.

The physics is simple: the Higgs masses at the GUT scale start with a value of $\sqrt{m_0^2 + \mu^2}$ and EWSB requires at least one of them to become negative at the electroweak scale by radiative corrections, mainly from the Yukawa couplings of the third generation. This is only possible if the starting value is not too high, so a large value of m_0 has to be compensated by a low value of μ . This is demonstrated in Fig. 3, which shows that μ becomes small and the Higgsino component in the lightest neutralino becomes large for large values of m_0 .

The strong production cross sections are characterized by a large number of jets from long decay chains and missing energy from the escaping neutralino. These characteristics can be used to efficiently suppress the background. For the electroweak production, both the number of jets and the missing transverse energy is low, since the LSP is not boosted so strongly as in the decay of the heavier strongly interacting particles. Hence, the electroweak gaugino production needs leptonic decays to reduce the background, so these signatures need more luminosity and cannot compete at present with the sensitivity of the strong production of squarks and gluinos.

The total cross section for the strongly interacting particles are shown in Fig. 4 together with the excluded region from direct searches at the LHC for SUSY particles. One observes that the excluded region (below the solid line) follows rather closely the total cross section, indicated by the

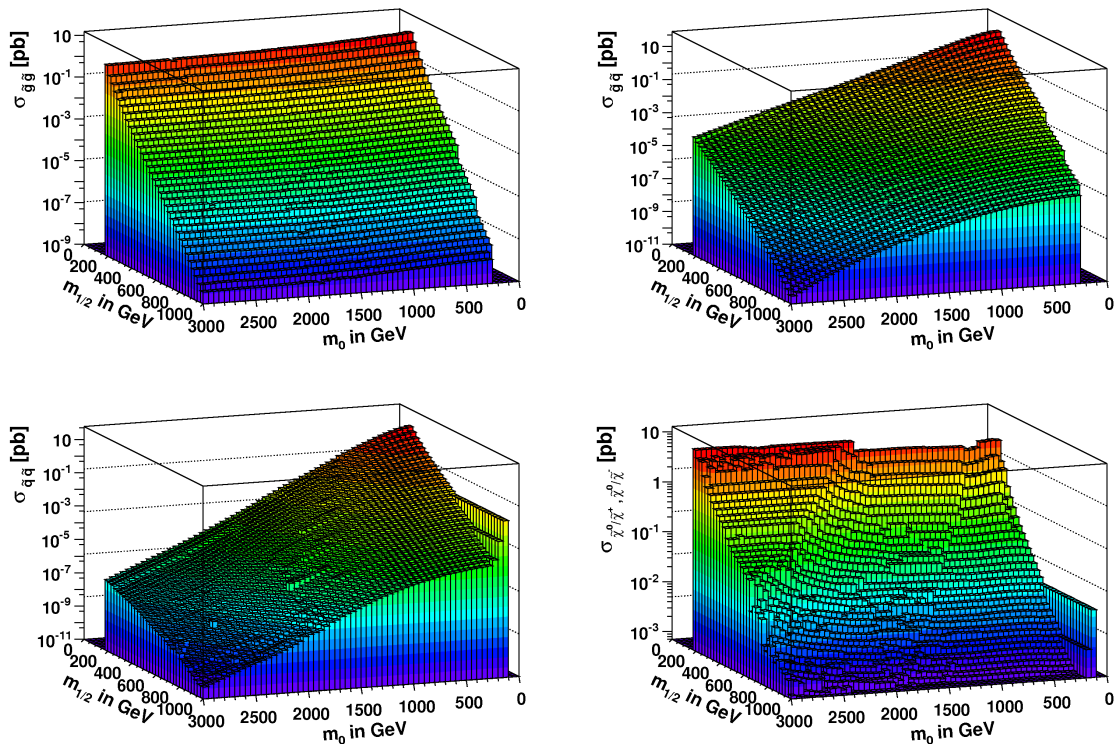


Figure 2: Cross sections for SUSY particle production for the diagrams shown in Fig. 1: clockwise via strong interactions ($\tilde{g}\tilde{g}$, $\tilde{g}\tilde{q}$ and $\tilde{q}\tilde{q}$, respectively) and electroweak interactions.

colour shading. From the colour coding one observes that the excluded region corresponds to a cross section limit of about 0.1 -0.2 pb. The excluded region was obtained by combining the ATLAS [5] and CMS [6] limits in the following way. Since the excluded region follows rather closely the total cross section the χ^2 contribution has been parametrized as $\sigma_{tot}^2/\sigma_{eff}^2$, where σ_{eff}^2 can be determined by requiring that for each point in the m_0 , $m_{1/2}$ plane the χ^2 value corresponds to an UP-parameter of $\chi^2 - \chi_{min}^2 = 5.99$, which corresponds to a 95% confidence level for a two-dimensional parameter space² [45]. Determining the parameter σ_{eff}^2 for each point of the contour and each experiment independently implies that our contours are identical to the contours given by the experiments. Then the χ^2 contributions are simply added, assuming no correlation between the experiments. If the LHC data is combined with cosmological and electroweak data, the fitted values of $\tan\beta$ and the trilinear coupling vary, while the LHC limits are given for fixed values $\tan\beta = 10$ and $A_0 = 0$. In our definition of χ^2 the cross section variations as function of these parameters are correctly taken into account under the assumption that the efficiency does not vary with these parameters, which is a good approximation for the hadronic searches. Therefore we only consider limits from LHC data based on jets and missing energy and do not include the less sensitive limits from leptonic data.

The drop of the excluded region at large values of m_0 is due to the fact that in this region the squarks become heavy, which means that the contributions from the diagrams in the second and third row of Fig. 1 start to diminish. Here only higher energies will help and doubling the LHC energy from 7 to 14 TeV, as planned in the coming years, quickly increases the cross section for gluino

²This UP-parameter is for a two-sided confidence interval. However, several observables, like the LHC limits, refer to a single-sided lower limit. For a single-sided limit the UP-parameter would be 4.61. We keep conservatively an UP-parameter of 5.99, which for a single-sided limit would correspond to a 97.5% confidence level. Because of the steeply falling cross section the difference between 95 and 97.5% is small for the exclusion line in the m_0 , $m_{1/2}$ plane.

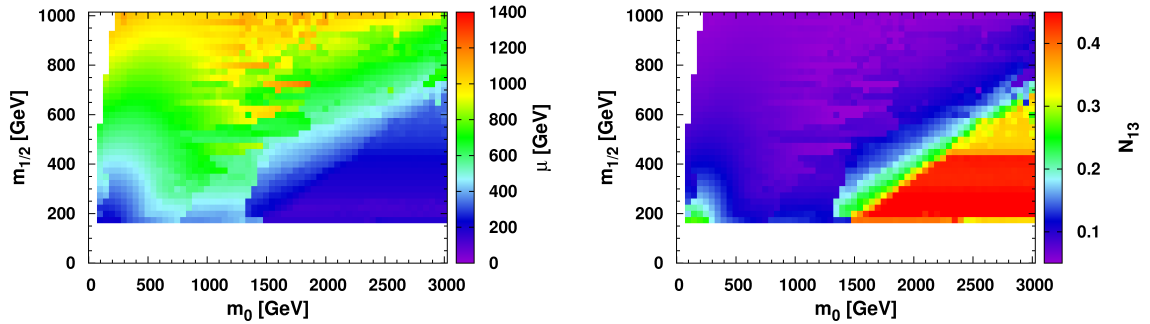


Figure 3: Values of μ and N_{13} in the $m_0, m_{1/2}$ plane. The strong decrease of μ and corresponding increase of N_{13} at large values of m_0 is largely determined by the EWSB constraint. Note that the right bottom corner is typically excluded by EWSB, *if* the trilinear coupling A_0 and $\tan \beta$ are fixed. However, if all parameters are left free in the fit, EWSB can be fulfilled in the whole region shown.

production by orders of magnitude, as shown in the right panel of Fig. 4. The expected sensitivity at 14 TeV, plotted as an exclusion contour in case nothing will be found, assumes the same efficiency and luminosity (slightly above one fb^{-1} per experiment) as at 7 TeV.

These limits can be translated to squark and gluino masses as follows. The squarks have a starting value at the GUT scale equal to m_0 , but have important contributions from gluinos in the colour field, so the squark masses are given by $m_q^2 \approx m_0^2 + 6.6m_{1/2}^2$, as was determined from the renormalization group equations [50]. Similarly the gluino mass is given by $2.7m_{1/2}$. The term proportional to $m_{1/2}$ in the squark mass corresponds to the self-energy diagrams, which imply that if the "gluino-cloud" is heavy, the squarks cannot be light. This leads to the regions indicated as not allowed in Fig. 5. Note that these regions are forbidden in any model with a coupling between squarks and gluinos, so they are not specific to the CMSSM. Squark masses below 1.1 TeV and gluino masses below 0.62 TeV are excluded for the LHC data at 7 TeV, as shown in the left panel of Fig. 5. Expected sensitivities for higher integrated luminosities at 7 and 14 TeV have been indicated as well. One observes that increasing the energy is much more effective than increasing the luminosity. At 14 TeV squark masses of 1.7 TeV and gluino masses of 1.02 TeV are within reach with one fb^{-1} per experiment, as shown in the right panel of Fig. 5.

3 Excluded region by the relic density

The observed relic density of DM corresponds to $\Omega h^2 = 0.113 \pm 0.004$ [4], which is about a factor six higher than the baryonic density. This number is inversely proportional to the annihilation cross section. The dominant annihilation contribution comes from A-boson exchange in most of the parameter space, if one excludes the narrow co-annihilation regions [43]. The cross section for $\chi + \chi \rightarrow A \rightarrow b\bar{b}$ can be written as:

$$\langle \sigma v \rangle \sim \frac{M_\chi^4 m_b^2 \tan^2 \beta (N_{31} \sin \beta - N_{41} \cos \beta)^2 (N_{21} \cos \theta_W - N_{11} \sin \theta_W)^2}{\sin^4 2\theta_W M_Z^2 (4M_\chi^2 - M_A^2)^2 + M_A^2 \Gamma_A^2}, \quad (1)$$

where the elements of the mixing matrix in the neutralino sector define the content of the lightest neutralino

$$|\tilde{\chi}_1^0\rangle = N_{11}|B_0\rangle + N_{12}|W_0^3\rangle + N_{13}|H_1\rangle + N_{14}|H_2\rangle. \quad (2)$$

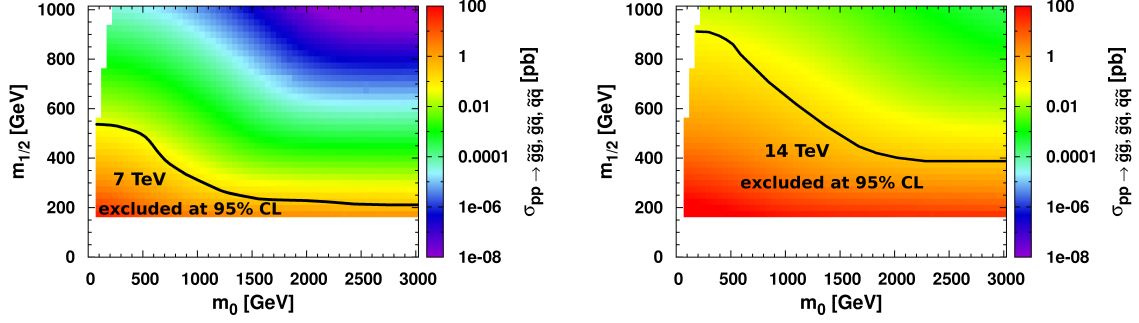


Figure 4: Left: Total production cross section of strongly interacting particles in comparison with the LHC excluded limits for 7 TeV. Here the data from ATLAS and CMS were combined and correspond to an integrated luminosity of 1.3 and 1.1 fb^{-1} , respectively. One observes that a cross section of 0.1 to 0.2 pb is excluded at 95% confidence level. Right: the cross sections at 14 TeV and expected exclusion for the same limit on the cross section as at 7 TeV (left panel).

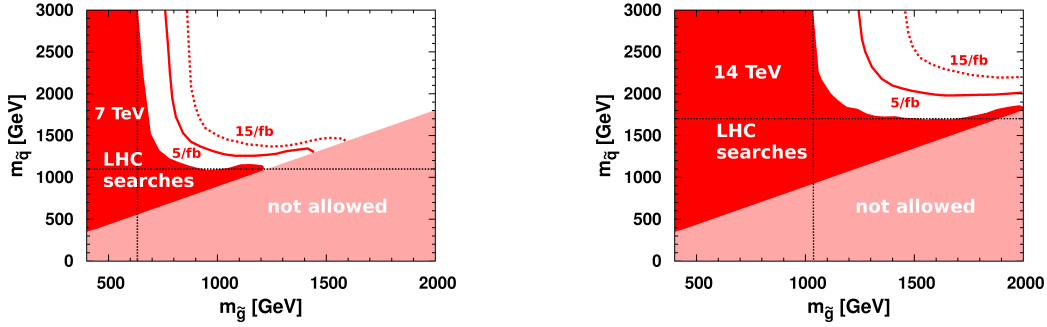


Figure 5: As in Fig. 4, but the excluded region is translated into the $m_{\tilde{q}}, m_{\tilde{g}}$ plane. The red area corresponds to excluded regions for an integrated luminosity slightly above $1/\text{fb}$; the expectations for higher luminosities have been indicated as well. Note that the regions indicated as not allowed are not a feature of the CMSSM, but are valid in any model, which has a coupling between squarks and gluinos, which lead to self-energy diagrams of the squarks. These imply that if the "gluino-cloud" is heavy, the squarks cannot be light.

The correct relic density requires $\langle \sigma v \rangle = 2 \cdot 10^{-26} \text{ cm}^3/\text{s}$, which implies that the annihilation cross section σ is of the order of a few pb. Such a high cross section can be obtained only close to the resonance. Actually on the resonance the cross section is too high, so one needs to be in the tail of the resonance, i.e. $m_A \approx 2.2m_\chi$ or $m_A \approx 1.8m_\chi$. So one expects $m_A \propto m_{1/2}$ from the relic density constraint. This constraint can be fulfilled with $\tan\beta$ values around 50 in the whole $m_0, m_{1/2}$ plane, except for the narrow co-annihilation regions, as we showed previously [43]. The results were extended to larger values of m_0 , as shown in the left panel of Fig. 6. The rather strong limits on the pseudo-scalar Higgs boson from LHC [51, 52], especially at large values of $\tan\beta$, lead then to constraints on $m_{1/2}$ of about 400 GeV for intermediate values of m_0 , as shown in the right panel of Fig. 6. Note that the top left corner (white) is not allowed, because in this region of small m_0 and large $m_{1/2}$ the stau

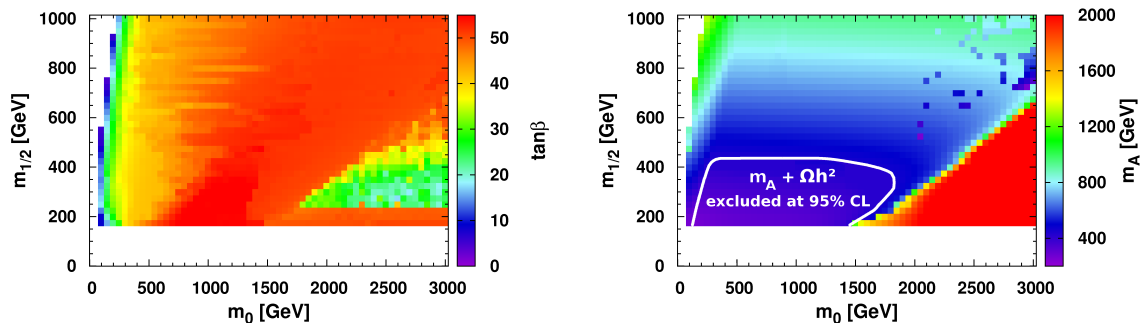


Figure 6: Fitted values of $\tan\beta$ (left) and constraint from relic density combined with the pseudo-scalar Higgs limit (right) in the $m_0, m_{1/2}$ plane after optimizing $\tan\beta$ and A_0 to fulfill the relic density and EWSB constraints at every point. The relic density requires $\tan\beta \approx 50$ in most of the parameter space, where pseudo-scalar Higgs exchange dominates. In the (non-red) edges where $\tan\beta$ is lower, co-annihilation contributes. The data below the solid line in the right panel is excluded at 95 % confidence level.

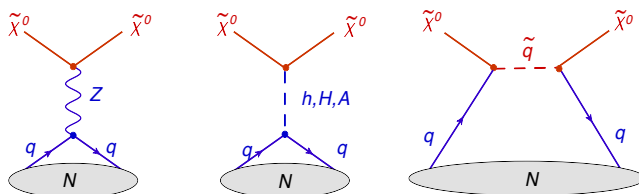


Figure 7: Examples of diagrams for elastic neutralino-nucleon scattering.

becomes the lightest supersymmetric particle (LSP). However, a charged LSP cannot be the DM. As will be shown later in Fig. 10, for even larger values of $m_{1/2}$ this non-allowed region becomes broader, while the relic density requires large $\tan\beta$ away from the co-annihilation region, in which case the mixing in the stau sector increases and the stau becomes again the LSP.

4 Excluded region by direct DM searches

Scattering of LSPs on nuclei can only happen via elastic scattering, if R-parity is conserved [1, 2]. The corresponding diagrams are shown in Fig. 7. The big blob indicates that one enters a low energy regime, in which case the protons and neutrons inside the nucleus cannot be resolved. In this case the spin independent scattering becomes coherent on all nuclei and the cross section becomes proportional to the number of nuclei:

$$\sigma = \frac{4}{\pi} \frac{m_{\text{DM}}^2 m_N^2}{(m_{\text{DM}} + m_N)^2} (Z f_p + (A - Z) f_n)^2 \quad (3)$$

where A and Z are the atomic mass and atomic number of the target nuclei. Since the particle which mediates the scattering is typically much heavier than the momentum transfer, the scattering can be written in terms of an effective coupling. Using the notation of Ref. [53] one can write:

$$f_{p,n} = \sum_{q=u,d,s} G_q f_{Tq}^{(p,n)} \frac{m_{p,n}}{m_q} + \frac{2}{27} f_{TG}^{(p,n)} \sum_{q=c,b,t} G_q \frac{m_{p,n}}{m_q}, \quad (4)$$

where $G_q = \lambda_{\text{DM}}\lambda_q/M_M^2$. Here M denotes the mediator, and $\lambda_{\text{DM}}, \lambda_f$ denote the mediator's couplings to DM and quark. The parameters $f_{Tq}^{(p)}$ are defined by

$$m_p f_{Tq}^{(p)} \equiv \langle p | m_q \bar{q}q | p \rangle \quad (5)$$

and similar for $f_{Tq}^{(n)}$, whilst $f_{TG}^{(p,n)} = 1 - \sum_{q=u,d,s} f_{Tq}^{(p,n)}$.

When squarks become heavy, the squark exchange diagram in Fig. 7 becomes suppressed and the only relevant mediator is the Higgs boson, in which case the heavier sea quarks in the sum in Eq. 4 become the main contributor to the elastic cross section. Remember that the coupling between the Higgs and down-type quarks is additionally enhanced by $\tan\beta$ [22, 54], so the charm and top contributions are suppressed for the large values of $\tan\beta$ in Fig. 6.

The scalar density of the heavy quarks can be inferred from the nucleon masses, since a large density of heavy quarks would increase the nucleon mass. The nucleon mass can be written as $M_N = M_0 + \sigma_{\pi N}$, where M_0 is the nucleon mass in the chiral limit and $\sigma_{\pi N}$ characterizes the effect of the finite quark masses. The u, d quarks contribute both as valence and sea quarks, while the heavier quarks contribute only as sea quarks. The strange quark content is usually parametrized by the y -parameter:

$$y = \frac{2\langle N | s\bar{s} | N \rangle}{\langle N | u\bar{u} + d\bar{d} | N \rangle}.$$

Phenomenologically, the πN scattering is related to the $\sigma_{\pi N}$ term, while the contribution of heavier quarks is related to the octet breaking of the baryon masses. From these data one obtains $y=0.3-0.6$ [55]. Such large values are surprising, but one should keep in mind that they originate from the gluon splitting inside a proton, which is the non-perturbative regime of QCD and the interpretations might be prone to higher order corrections.

An alternative solution for calculating the scalar quark densities in the non-perturbative regime is provided by lattice QCD. Such calculations allow to determine the valence and sea quark distributions to the $\sigma_{\pi N}$ independently. After imposing the chiral symmetry in the lattice calculations the authors of Ref. [55] find that the valence quarks dominate the $\sigma_{\pi N}$ term and the y parameter is small (< 0.05).

The default values of the effective couplings in Eq. 5 are in micrOMEGAs [56]: $f_{Tu}^{(p)} = 0.033$, $f_{Td}^{(p)} = 0.023$, $f_{Ts}^{(p)} = 0.26$, $f_{Tu}^{(n)} = 0.042$, $f_{Td}^{(n)} = 0.018$, $f_{Ts}^{(n)} = 0.26$. If one takes the lower y values from the lattice calculations one finds [57]: $f_{Tu}^{(p)} = 0.020$, $f_{Td}^{(p)} = 0.026$, $f_{Ts}^{(p)} = 0.02$, $f_{Tu}^{(n)} = 0.014$, $f_{Td}^{(n)} = 0.036$, $f_{Ts}^{(n)} = 0.02$. So the most important coupling to the strange quarks is reduced from 0.26 to 0.02, which implies an order of magnitude uncertainty in the elastic neutralino-nucleon scattering cross section.

Another normalization uncertainty in direct dark matter experiments arises from the uncertainty in the local DM density, which can take values between 0.3 and 1.3 GeV/cm³, as determined from the rotation curve of the Milky Way, see Ref. [58, 59] and references therein.

These overall normalization uncertainties from the scalar quarks densities inside the nucleon and the DM densities in the Galaxy are independent of the SUSY parameter space. However, the effective couplings vary strongly inside the SUSY parameter space.

The scattering cross section is proportional to the product of gaugino and Higgsino components squared [22, 54], so it rises rapidly, if the Higgsino component increases, which is the case for large values of m_0 , as shown before in Fig. 3. To get conservative estimates for the excluded regions, we take the lowest possible values of the local DM density and the couplings. The difference in couplings is the largest contributor to the uncertainty and the difference in excluded regions is demonstrated in Fig. 8 (left panel). The dotted line corresponds to the default micrOMEGAs values of the couplings based on the $\sigma_{\pi N}$ term from data, while the dashed-dotted line indicates the 95% excluded region using the smaller and hence more conservative couplings from lattice gauge theory. The colours indicate the $\Delta\chi^2 = \chi^2 - \chi_{\text{min}}^2$ contribution from the electroweak constraints: $b \rightarrow X_s\gamma = (3.55 \pm 0.24) \cdot 10^{-4}$ [60],

g-2 [61], $B_s^0 \rightarrow \mu^+\mu^- < 1.1 \cdot 10^{-8}$ [62], $B_u \rightarrow \tau\nu = (1.68 \pm 0.31) \cdot 10^{-4}$ [60], $m_h > 114.4$ GeV [63]. $\chi_{min} = 2.5$ in this plot for two degrees of freedom, if we consider only the measured values (excluding limits) minus the two fitted SUSY parameters A_0 and $\tan\beta$.

If we combine all constraints one finds that $m_{1/2}$ below 400 GeV is excluded for all values of m_0 , as shown in the right panel of Fig. 8. At low values of m_0 the direct searches dominate the limit, as shown previously in Fig. 4. At intermediate values of m_0 the relic density constraint dominates the limit, as shown in Fig. 6, while at large values the limit is dominated by the XENON100 data (Fig. 8, left panel).

It should be noted that these combined limits from the LHC, WMAP and XENON100 are stronger than the limits from the LEP Higgs limits, electroweak and b-physics observables (red area in Fig. 8, left), so these hardly play a role anymore. Only g-2 yields a mild, but insignificant preference for low values of m_0 , especially if one combines the non-Gaussian theoretical errors linearly with the experimental errors. This will be discussed in more detail below.

4.1 Discussion on g-2

The theoretical value of g-2 has been reviewed in Ref. [64], which is still in agreement with the latest values from Ref. [65]. We use the difference Δa_μ in g-2 between the experimental and theoretical value as input to the χ^2 value and use $\Delta a_\mu = 302 \pm 63(exp) \pm 61(theo.) \cdot 10^{-11}$, so the theoretical and experimental errors are similar. The theoretical error from the light-by-light scattering contribution alone is 26, so this error dominates, but it has certainly not a Gaussian distribution. For non-Gaussian errors, especially errors with an equal probability in a certain interval, it is more conservative to add the errors linearly, as can be tested by simply comparing the convolution of two Gaussians with a Gaussian and a "flat top" Gaussian, where the flat region represents the interval with a constant probability. In the first case one finds the usual result that the probability distribution from the combined uncertainties equals a Gaussian with the errors added in quadrature, while in the second case the probability distribution equals a Gaussian with an error closer to the linear addition of the individual errors. To be conservative we have added the theoretical and experimental errors linearly, which increases the error for g-2 from 88 to 124 in units of 10^{-11} , so the χ^2 contribution is reduced by about a factor two, but there is still a preferred region with lower χ^2 , as shown in Fig. 9, left panel. To be consistent we have added theoretical and experimental errors linearly for all other observables as well.

If we exclude g-2, the remaining observables are insensitive to the region with large SUSY masses, as can be seen from the flat χ^2 distribution in the right panel of Fig. 9, which can be compared with the right panel of Fig. 8, where g-2 was included. One observes that the XENON100 limit excludes $m_{1/2} < 300$ GeV for large m_0 , but if combined with g-2 the exclusion goes up to 400 GeV in this region.

5 Summary

If one combines the excluded region from the direct searches at the LHC (Fig. 4, left) and the relic density from WMAP combined with the already stringent limits on the pseudo-scalar Higgs mass (Fig. 6) with the XENON100 limits (Fig. 8, left) one obtains the excluded region shown in the right panel of Fig. 8. Here the g-2 limit is included with the conservative linear addition of theoretical and experimental errors. One observes that the combination excludes $m_{1/2}$ below 400 GeV for all values of m_0 , which implies the LSP has to have masses above 160 GeV within the CMSSM from the constraints considered. The gluino mass has to be above 1 TeV in this case.

As discussed in Sect. 2, the LHC becomes rather insensitive to the large m_0 region because of the decreasing cross section for the production of strongly interaction particles and the large background for the production of gauginos. However, in this region one obtains an increased sensitivity above

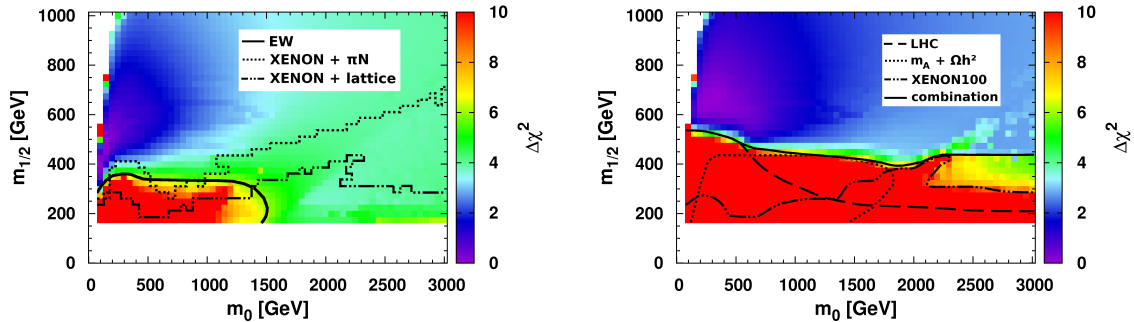


Figure 8: Left: $\Delta\chi^2 = \chi^2 - \chi_{min}^2$ distribution in the $m_0, m_{1/2}$ plane after imposing the electroweak constraints in comparison with the XENON100 limits [19] on the direct WIMP-nucleon cross section for two values of the form factors (dotted line: πN scattering, dashed dotted line: lattice gauge theories). Values with $\Delta\chi^2 = \chi^2 - \chi_{min}^2 > 5.99$ are excluded (red region). $\chi_{min}^2 = 2.5$ for two degrees of freedom. Right: as left after imposing the combined constraints from LHC, WMAP, electroweak constraints and XENON100. $\chi_{min}^2 = 3.6$ for two degrees of freedom, which is slightly higher than in the left panel because of the increased contribution from g-2, see Fig. 9.

the LHC limits from relic density and direct DM searches for two reasons. First, the relic density is inversely proportional to the annihilation rate, which leads to an annihilation cross section of the order of a few pb. Such a large cross section can only be obtained by annihilation via pseudo-scalar Higgs boson exchange in the s-channel in most of the parameter space. The mass of the pseudo-scalar Higgs boson can be tuned everywhere in the $m_0, m_{1/2}$ plane by choosing the correct value of $\tan\beta$, which has to be around 50 in this case. Such a large value of $\tan\beta$ leads to a large pseudo-scalar Higgs boson cross section at the LHC, since it is proportional to $\tan\beta^2$. The LHC limit on the pseudo-scalar Higgs mass leads to a lower limit on $m_{1/2}$ of 400 GeV for intermediate values of m_0 , as shown in Fig. 6.

Secondly, the cross section for direct scattering of WIMPS on nuclei has an upper limit of about 10^{-8} pb, i.e. many orders of magnitude below the annihilation cross section. These cross sections are related to each other by the diagrams and kinematics. The many orders of magnitude are naturally explained in Supersymmetry by the fact that both cross sections are dominated by Higgs exchange and the fact that the Yukawa couplings to the valence quarks in the proton or neutron are negligible. Most of the scattering cross section comes from the heavier sea-quarks. However, the density of these virtual quarks inside the nuclei is small, which is one of the reasons for the small elastic scattering cross section. In addition, the momentum transfer is small, so the propagator leads to a cross section inversely proportional to the fourth power of the Higgs mass. At large values of m_0 EWSB forces the Higgsino component of the WIMP to increase and consequently the exchange via the Higgs, which has an amplitude proportional to the bino-Higgsino mixing, starts to increase. This leads to an increase in the excluded region at large m_0 .

As mentioned in the introduction, several groups have performed similar analysis. Our results are closest to the one of Ref. [31]. They define the limits within the frequentist approach in a similar way as we do. Instead of optimizing the SUSY parameters by calculating the observables during execution of the program, they prepare a large data base of randomly sampled SUSY points with the observables calculated at each point. The results for small values of $m_{1/2}$ are similar to ours, although they use cross sections for the XENON100 results with couplings intermediate between the πN scattering and lattice gauge theories, while we used conservatively the lattice gauge theories. The

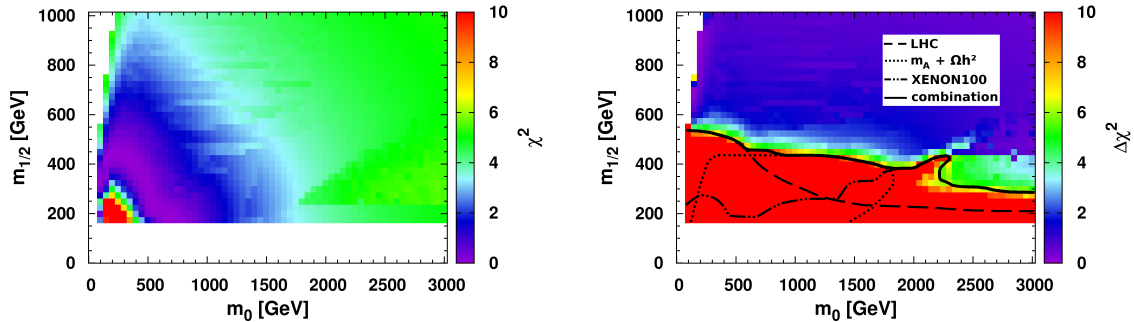


Figure 9: Left: $\Delta\chi^2 = \chi^2 - \chi_{min}^2$ distribution of the g-2 observable alone under the constraint that $\tan\beta$ and A_0 are still fixed by all other constraints. One observes a shallow increase of the χ^2 value for large SUSY masses, because g-2 prefers light SUSY particles. Right: the total $\Delta\chi^2$ distribution without g-2 constraint. One observes that all points above the excluded region (solid line) are equally probable. Note that the combined limit is slightly reduced at large values of m_0 in comparison with Fig. 8, right panel, while g-2 still contributes, even if the errors are added linearly.

difference between πN scattering and lattice gauge theories has been displayed in the left panel of Fig. 8. They display results up to $m_{1/2} = 2500$ GeV, since they find excluded regions above this value, which is due to the relic density constraint [66]. In our case we do find good solutions and no excluded region is found above $m_{1/2} = 400$ GeV, as shown in Fig. 10, left panel. This is probably due to the fact that in this region $\tan\beta$ and A_0 are highly correlated, so they can be easily missed in randomly chosen SUSY samples. The strong correlation is shown in the right panel of Fig. 10 and the best solutions are obtained close to the white stripes at the top and bottom, which are near the stau co-annihilation region. In the white region the stau is the LSP. As shown in the right panel of Fig. 10 there is no preferred region above $m_{1/2} = 400$ GeV, if g-2 is excluded and the region where the stau becomes the LSP is ignored. The preferred minimum for g-2 (around $m_0 = 400, m_{1/2} = 200$ GeV (Fig. 9 left) is already excluded by the LHC data and the slight preference above $m_{1/2} = 400$ is solely due to the shallow tail in the χ^2 distribution of g-2 (Fig. 9, left panel). How strong this preference is depends then on the treatment of the errors of g-2. As argued above the theoretical errors of the light-by-light scattering dominate and are certainly non-Gaussian, in which case a linear addition of the experimental and theoretical errors is the more conservative approach, so we do not think the preference by the region selected by g-2 and the corresponding preference for the expected SUSY masses is worth emphasizing in contrast to Ref. [31].

Our results differ significantly from results using Markov Chain Monte Carlo sampling. E.g. in Ref. [32] values for intermediate values of m_0 are excluded, which is the region of large $\tan\beta$ (see Fig. 6, left panel). Here the parameters $\tan\beta$ and A_0 are highly correlated again (Fig. 10, right panel) and finding the correct minimum depends strongly on the stepping algorithm, e.g. stepping in the logarithm of a parameter is different from stepping in the parameter ("prior dependence"). Such dependence on sampling techniques largely disappears in our multistep fitting technique, since for each point of the $m_0, m_{1/2}$ grid a unique solution is found independent of the minimizer used, so the frequentist approach with χ^2 minimization yields the same results as a likelihood optimization with a Markov Chain sampling technique.

If one combines the limits from the direct searches at the LHC, heavy flavour constraints, WMAP and XENON100 using the most conservative assumptions of linear addition of theoretical and experimental errors and the lowest local relic density and matrix elements for the XENON100 limit we

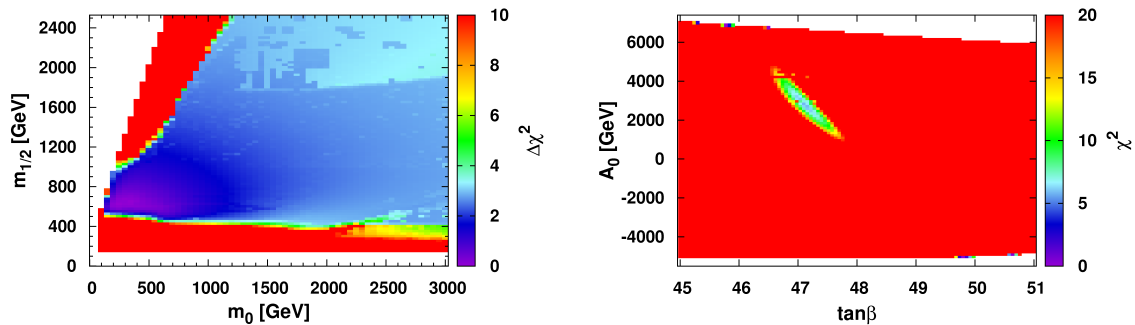


Figure 10: Left: $\Delta\chi^2$ distribution of all constraints up to $m_{1/2} = 2500$ GeV, showing that the χ^2 does not increase because of the relic density for large neutralino masses in contrast to Ref. [31]. The white region in the top left corner is excluded because the stau is always the LSP. The red region in this corner is excluded by the relic density constraint requiring large $\tan\beta$, which in turn cause a large mixing in the stau sector leading to the stau becoming the LSP again. Right: $\tan\beta$ and A_0 are strongly correlated for large neutralino masses by the relic density constraint; here $m_0 = 2500$ GeV and $m_{1/2} = 2000$ GeV has been chosen as an example.

exclude values of $m_{1/2}$ below 400 GeV in the CMSSM *independent* of m_0 , which implies a lower limit on the WIMP mass of 160 GeV and a gluino mass above 1 TeV. This is the CMSSM parameter region, where SUSY can be found.

Note that the CMSSM relates electroweak gauginos and gluinos by requiring gaugino mass unification. However, the squark and gluino masses are related by the squark self-energy diagrams, which are valid in any model with couplings between squarks and gluinos. So the gluino limits from Fig. 5 of 620 GeV are model-independent.

6 Acknowledgements

Support from the Deutsche Forschungsgemeinschaft (DFG) via a Mercator Professorship (Prof. Kazakov) and the Graduiertenkolleg "Hochenergiephysik und Teilchenastrophysik" in Karlsruhe is greatly appreciated. Furthermore, support from the Bundesministerium für Bildung und Forschung (BMBF) is acknowledged. We thank A. Phukov for help in calculating the SUSY cross section with CalcHEP inside micrOMEGAs.

References

- [1] E. W. Kolb and M. S. Turner, "The Early universe", *Front.Phys.* **69** (1990) 1–547.
- [2] G. Jungman, M. Kamionkowski, and K. Griest, "Supersymmetric dark matter", *Phys.Rept.* **267** (1996) 195–373, [arXiv:hep-ph/9506380](#).
- [3] G. Bertone, D. Hooper, and J. Silk, "Particle dark matter: Evidence, candidates and constraints", *Phys.Rept.* **405** (2005) 279–390, [arXiv:hep-ph/0404175](#).
- [4] E. Komatsu et al., "Seven-Year Wilkinson Microwave Anisotropy Probe (WMAP) Observations: Cosmological Interpretation", *Astrophys.J.Suppl.* **192** (2011) 18, [arXiv:1001.4538](#).

- [5] ATLAS Collaboration, “Search for new phenomena in final states with large jet multiplicities and missing transverse momentum using $\sqrt{s}=7$ TeV pp collisions with the ATLAS detector”, *JHEP* **1111** (2011) 099, [arXiv:1110.2299](#).
- [6] CMS Collaboration, “Search for Supersymmetry at the LHC in Events with Jets and Missing Transverse Energy”, *Phys.Rev.Lett.* **107** (2011) 221804, [arXiv:1109.2352](#).
- [7] CMS Collaboration, “Search for Supersymmetry in pp Collisions at 7 TeV in Events with Jets and Missing Transverse Energy”, *Phys.Lett.* **B698** (2011) 196–218, [arXiv:1101.1628](#).
- [8] CMS Collaboration, “Search for Supersymmetry in Events with b Jets and Missing Transverse Momentum at the LHC”, *JHEP* **1107** (2011) 113, [arXiv:1106.3272](#).
- [9] CMS Collaboration, “Search for New Physics with Jets and Missing Transverse Momentum in pp collisions at $\sqrt{s} = 7$ TeV”, *JHEP* **1108** (2011) 155, [arXiv:1106.4503](#).
- [10] CMS Collaboration, “Search for supersymmetry in pp collisions at 7 TeV in events with a single lepton, jets, and missing transverse momentum”, [arXiv:1107.1870](#). * Temporary entry *.
- [11] CMS Collaboration, “Search for supersymmetry in events with a lepton, a photon, and large missing transverse energy in pp collisions at $\sqrt{s} = 7$ TeV”, *JHEP* **1106** (2011) 093, [arXiv:1105.3152](#).
- [12] CMS Collaboration, “Search for new physics with same-sign isolated dilepton events with jets and missing transverse energy at the LHC”, *JHEP* **1106** (2011) 077, [arXiv:1104.3168](#).
- [13] CMS Collaboration, “Search for Supersymmetry in pp Collisions at $\sqrt{s} = 7$ TeV in Events with Two Photons and Missing Transverse Energy”, *Phys.Rev.Lett.* **106** (2011) 211802, [arXiv:1103.0953](#).
- [14] CMS Collaboration, “Search for Physics Beyond the Standard Model Using Multilepton Signatures in pp Collisions at $\sqrt{s}=7$ TeV”, *Phys.Lett.* **B704** (2011) 411–433, [arXiv:1106.0933](#).
- [15] ATLAS Collaboration, “Search for supersymmetry using final states with one lepton, jets, and missing transverse momentum with the ATLAS detector at 7 TeV”, *Phys.Rev.Lett.* **106** (2011) 131802, [arXiv:1102.2357](#).
- [16] ATLAS Collaboration, “Search for supersymmetric particles in events with lepton pairs and large missing transverse momentum in $\sqrt{s} = 7$ TeV proton-proton collisions with the ATLAS experiment”, *Eur.Phys.J.* **C71** (2011) 1682, [arXiv:1103.6214](#).
- [17] ATLAS Collaboration, “Search for supersymmetry in pp collisions at $\sqrt{s} = 7$ TeV in final states with missing transverse momentum and b-jets”, *Phys.Lett.* **B701** (2011) 398–416, [arXiv:1103.4344](#).
- [18] Z. Ahmed et al., “Combined Limits on WIMPs from the CDMS and EDELWEISS Experiments”, *Phys.Rev.* **D84** (2011) 011102, [arXiv:1105.3377](#).
- [19] E. Aprile et al., “Dark Matter Results from 100 Live Days of XENON100 Data”, *Phys.Rev.Lett.* **107** (2011) 131302, [arXiv:1104.2549](#).
- [20] A. H. Chamseddine, R. L. Arnowitt, and P. Nath, “Locally Supersymmetric Grand Unification”, *Phys.Rev.Lett.* **49** (1982) 970.

- [21] C. F. Kolda, L. Roszkowski, J. D. Wells et al., “Predictions for constrained minimal supersymmetry with bottom tau mass unification”, *Phys.Rev.* **D50** (1994) 3498–3507, [arXiv:hep-ph/9404253](#).
- [22] H. E. Haber and G. L. Kane, “The Search for Supersymmetry: Probing Physics Beyond the Standard Model”, *Phys.Rept.* **117** (1985) 75–263.
- [23] W. de Boer, “Grand unified theories and supersymmetry in particle physics and cosmology”, *Prog.Part.Nucl.Phys.* **33** (1994) 201–302, [arXiv:hep-ph/9402266](#).
- [24] S. P. Martin, “A Supersymmetry primer”, [arXiv:hep-ph/9709356](#).
- [25] D. Kazakov, “Supersymmetry on the Run: LHC and Dark Matter”, *Nucl.Phys.Proc.Suppl.* **203-204** (2010) 118–154, [arXiv:1010.5419](#).
- [26] U. Amaldi, W. de Boer, and H. Furstenau, “Comparison of grand unified theories with electroweak and strong coupling constants measured at LEP”, *Phys.Lett.* **B260** (1991) 447–455.
- [27] K. Inoue, A. Kakuto, H. Komatsu et al., “Aspects of Grand Unified Models with Softly Broken Supersymmetry”, *Prog.Theor.Phys.* **68** (1982) 927.
- [28] A. Gladyshev, D. Kazakov, W. de Boer et al., “MSSM predictions of the neutral Higgs boson masses and LEP-2 production cross-sections”, *Nucl.Phys.* **B498** (1997) 3–27, [arXiv:hep-ph/9603346](#).
- [29] W. de Boer, M. Huber, C. Sander et al., “A global fit to the anomalous magnetic moment, $b \rightarrow X/s\gamma$ and Higgs limits in the constrained MSSM”, *Phys.Lett.* **B515** (2001) 283–290.
- [30] O. Buchmueller, R. Cavanaugh, D. Colling et al., “Supersymmetry and Dark Matter in Light of LHC 2010 and Xenon100 Data”, *Eur.Phys.J.* **C71** (2011) 1722, [arXiv:1106.2529](#).
- [31] O. Buchmueller, R. Cavanaugh, A. De Roeck et al., “Supersymmetry in Light of 1/fb of LHC Data”, [arXiv:1110.3568](#).
- [32] G. Bertone, D. Cerdeno, M. Fornasa et al., “Global fits of the cMSSM including the first LHC and XENON100 data”, *JCAP* **1201** (2012) 015, [arXiv:1107.1715](#).
- [33] B. Allanach, “Impact of CMS Multi-jets and Missing Energy Search on CMSSM Fits”, *Phys.Rev.* **D83** (2011) 095019, [arXiv:1102.3149](#).
- [34] B. Allanach, T. Khoo, C. Lester et al., “The impact of the ATLAS zero-lepton, jets and missing momentum search on a CMSSM fit”, *JHEP* **1106** (2011) 035, [arXiv:1103.0969](#).
- [35] M. Farina, M. Kadastik, D. Pappadopulo et al., “Implications of XENON100 and LHC results for Dark Matter models”, *Nucl.Phys.* **B853** (2011) 607–624, [arXiv:1104.3572](#).
- [36] A. Strumia, “Implications of first LHC results”, [arXiv:1107.1259](#).
- [37] S. Akula, D. Feldman, Z. Liu et al., “New Constraints on Dark Matter from CMS and ATLAS Data”, *Mod.Phys.Lett.* **A26** (2011) 1521–1535, [arXiv:1103.5061](#).
- [38] R. Trotta, F. Feroz, M. P. Hobson et al., “The Impact of priors and observables on parameter inferences in the Constrained MSSM”, *JHEP* **0812** (2008) 024, [arXiv:0809.3792](#).
- [39] Y. Akrami, P. Scott, J. Edsjo et al., “A Profile Likelihood Analysis of the Constrained MSSM with Genetic Algorithms”, *JHEP* **1004** (2010) 057, [arXiv:0910.3950](#).

- [40] F. Feroz, B. C. Allanach, M. Hobson et al., “Bayesian Selection of sign(μ) within mSUGRA in Global Fits Including WMAP5 Results”, *JHEP* **0810** (2008) 064, [arXiv:0807.4512](#).
- [41] S. Sekmen, S. Kraml, J. Lykken et al., “Interpreting LHC SUSY searches in the phenomenological MSSM”, [arXiv:1109.5119](#).
- [42] F. Feroz, K. Cranmer, M. Hobson et al., “Challenges of Profile Likelihood Evaluation in Multi-Dimensional SUSY Scans”, *JHEP* **1106** (2011) 042, [arXiv:1101.3296](#). 21 pages, 9 figures, 1 table/ minor changes following referee report. Matches version accepted by JHEP.
- [43] C. Beskidt et al., “Constraints on Supersymmetry from Relic Density compared with future Higgs Searches at the LHC”, *Phys. Lett.* **B695** (2011) 143–148, [arXiv:1008.2150](#).
- [44] C. Beskidt, W. de Boer, D. Kazakov et al., “Constraints from the decay $B_s^0 \rightarrow \mu^+ \mu^-$ and LHC limits on Supersymmetry”, *Phys.Lett.* **B705** (2011) 493–497, [arXiv:1109.6775](#).
- [45] F. James and M. Roos, “Minuit: A System for Function Minimization and Analysis of the Parameter Errors and Correlations”, *Comput.Phys.Commun.* **10** (1975) 343–367.
- [46] Particle Data Group Collaboration, “Review of particle physics”, *J.Phys.G* **G37** (2010) 075021.
- [47] G. Belanger, F. Boudjema, A. Pukhov et al., “micrOMEGAs: A Tool for dark matter studies”, [arXiv:1005.4133](#).
- [48] A. Pukhov, G. Belanger, F. Boudjema et al., “Tools for Dark Matter in Particle and Astroparticle Physics”, *PoS ACAT2010* (2010) 011, [arXiv:1007.5023](#).
- [49] A. Djouadi, J.-L. Kneur, and G. Moultaka, “SuSpect: A Fortran code for the supersymmetric and Higgs particle spectrum in the MSSM”, *Comput.Phys.Commun.* **176** (2007) 426–455, [arXiv:hep-ph/0211331](#).
- [50] W. de Boer, R. Ehret, and D. Kazakov, “Predictions of SUSY masses in the minimal supersymmetric grand unified theory”, *Z.Phys.* **C67** (1995) 647–664, [arXiv:hep-ph/9405342](#).
- [51] CMS Collaboration, “Search for Neutral MSSM Higgs Bosons Decaying to Tau Pairs in pp Collisions at $\sqrt{s} = 7$ TeV”, *Phys.Rev.Lett.* **106** (2011) 231801, [arXiv:1104.1619](#).
- [52] ATLAS Collaboration, “Search for neutral MSSM Higgs bosons decaying to tau tau pairs in proton-proton collisions at 7 TeV with the ATLAS detector”, [arXiv:1107.5003](#). * Temporary entry *.
- [53] J. R. Ellis, K. A. Olive, and C. Savage, “Hadronic Uncertainties in the Elastic Scattering of Supersymmetric Dark Matter”, *Phys.Rev.* **D77** (2008) 065026, [arXiv:0801.3656](#).
- [54] J. Gunion and H. E. Haber, “Higgs Bosons in Supersymmetric Models. 1.”, *Nucl.Phys.* **B272** (1986) 1.
- [55] H. Ohki, H. Fukaya, S. Hashimoto et al., “Nucleon sigma term and strange quark content from lattice QCD with exact chiral symmetry”, *Phys.Rev.* **D78** (2008) 054502, [arXiv:0806.4744](#).
- [56] G. Belanger, F. Boudjema, A. Pukhov et al., “Dark matter direct detection rate in a generic model with micrOMEGAs 2.2”, *Comput.Phys.Commun.* **180** (2009) 747–767, [arXiv:0803.2360](#).

- [57] J. Cao, K.-i. Hikasa, W. Wang et al., “Constraints of dark matter direct detection experiments on the MSSM and implications on LHC Higgs search”, *Phys.Rev.* **D82** (2010) 051701, [arXiv:1006.4811](#).
- [58] M. Weber and W. de Boer, “Determination of the Local Dark Matter Density in our Galaxy”, *Astron.Astrophys.* **509** (2010) A25, [arXiv:0910.4272](#).
- [59] W. de Boer and M. Weber, “The Dark Matter Density in the Solar Neighborhood reconsidered”, *JCAP* **1104** (2011) 002, [arXiv:1011.6323](#).
- [60] “<http://www.slac.stanford.edu/xorg/hfag/rare/ichep10/radll/OUTPUT/TABLES/radll.pdf> updated August 2010”,.
- [61] Muon G-2 Collaboration Collaboration, “Final Report of the Muon E821 Anomalous Magnetic Moment Measurement at BNL”, *Phys.Rev.* **D73** (2006) 072003, [arXiv:hep-ex/0602035](#).
- [62] CMS, LHCb, and Coll., “Search for the rare decay $B_s^0 \rightarrow \mu^+ \mu^-$ at the LHC”, **LHCb-CONF-2011-047, CMS PAS BPH-11-019** (2011).
- [63] ALEPH Collaboration, DELPHI Collaboration, L3 Collaboration, OPAL Collaborations, LEP Working Group for Higgs Boson Searches Collaboration, “Search for neutral MSSM Higgs bosons at LEP”, *Eur.Phys.J.* **C47** (2006) 547–587, [arXiv:hep-ex/0602042](#).
- [64] F. Jegerlehner and A. Nyffeler, “The Muon g-2”, *Phys.Rept.* **477** (2009) 1–110, [arXiv:0902.3360](#).
- [65] M. Davier, A. Hoecker, B. Malaescu et al., “Reevaluation of the Hadronic Contributions to the Muon g-2 and to $\alpha(MZ)$ ”, *Eur.Phys.J.* **C71** (2011) 1515, [arXiv:1010.4180](#).
- [66] S. Heinemeyer, “private communication”,.